

Article

In Vitro Gastrointestinal Release of Chlorogenic Acid and Curcumin Co-Encapsulated in Double Emulsions with the Outer Interface Stabilized by Cellulose Nanocrystals

Javier Paredes-Toledo ¹, Javier Herrera ¹, Paulo Díaz-Calderón ^{2,3}, Paz Robert ⁴ and Begoña Giménez ^{1,*}

¹ Department of Food Science and Technology, Faculty of Technology, University of Santiago, Av. Víctor Jara 3769, Estación Central, Santiago 9170124, Chile; javier.paredes@usach.cl (J.P.-T.); javier.herrera.c@usach.cl (J.H.)

² Biopolymer Research & Engineering Laboratory (BIOPREL), Escuela de Nutrición y Dietética, Facultad de Medicina, Universidad de los Andes, Avda. Monseñor Álvaro del Portillo 12,455, Las Condes, Santiago 7620001, Chile; pdiaz@uandes.cl

³ Centro de Investigación e Innovación Biomédica, Facultad de Medicina, Universidad de los Andes, Avda. Monseñor Álvaro del Portillo 12,455, Las Condes, Santiago 7620001, Chile

⁴ Department of Food Science and Chemical Technology, Faculty of Chemical and Pharmaceutical Sciences, University of Chile, Santos Dumont 964, Independencia, Santiago 8380494, Chile; proberts@uchile.cl

* Correspondence: bego.gimenez@usach.cl

Abstract: A Pickering double emulsion (DE) with an outer (O:W₂) interface stabilized by cellulose nanocrystals (DE-CNC) was designed as a co-delivery systems for chlorogenic acid (CA) and curcumin, then compared with a control DE emulsion with an O:W₂ interface stabilized with sodium caseinate (DE-NaCas). DE-CNC was more resistant to creaming during storage (6.79%, day 42) and showed higher encapsulation efficiency (EE) of CA (>90%). Conversely, both DEs exhibited similarly high EE for curcumin (>97%). The ζ-potential values were highly negative in both DEs, but tended to be lower in DE-CNC due to the highly negative charge of the CNCs. DE-CNC allowed for a steady release of CA during the oral, gastric, and intestinal phases of digestion, while a total release of CA was already observed in the gastric phase in case of DE-NaCas. The bioaccessibility of CA was similar in both DEs (~57–58%). Curcumin was mainly released in the intestinal phase with both DEs, reaching slightly lower bioaccessibility values with DE-CNC. The use of CNCs as a stabilizer for the outer interface of DEs is a promising strategy to increase the stability and EE of these systems, providing oral co-delivery vehicles capable of releasing significantly bioactive compounds during the intestinal phase of digestion.

Keywords: cellulose nanocrystals; Pickering double emulsion; co-delivery; chlorogenic acid; curcumin; *in vitro* digestion



Citation: Paredes-Toledo, J.; Herrera, J.; Díaz-Calderón, P.; Robert, P.; Giménez, B. *In Vitro* Gastrointestinal Release of Chlorogenic Acid and Curcumin Co-Encapsulated in Double Emulsions with the Outer Interface Stabilized by Cellulose Nanocrystals. *Colloids Interfaces* **2024**, *8*, 24. <https://doi.org/10.3390/colloids8020024>

Academic Editor: Thodoris Karapantsios

Received: 19 February 2024

Revised: 25 March 2024

Accepted: 29 March 2024

Published: 9 April 2024



Copyright: © 2024 by the authors. Licensee MDPI, Basel, Switzerland. This article is an open access article distributed under the terms and conditions of the Creative Commons Attribution (CC BY) license (<https://creativecommons.org/licenses/by/4.0/>).

1. Introduction

Emulsions play an important role in various industries, including foods, pharmaceuticals, and cosmetics. However, their low kinetic stability is a critical factor influencing their shelf life, functionality, and performance [1]. Water-in-oil-in-water (W₁/O/W₂) double emulsions (DEs) are multicompartiment systems characterized by the dispersion of a water-in-oil (W₁/O) emulsion as droplets within an external aqueous phase (W₂). These emulsions offer an advantage over simple emulsions, since they can co-encapsulate hydrophilic bioactive compounds in the W₁ phase and hydrophobic ones in the oil phase [2]. This makes DEs a promising co-delivery system for the controlled release of both hydrophilic and hydrophobic bioactive compounds. Over the past few years, numerous hydrophilic and lipophilic bioactive compounds have been simultaneously encapsulated in DEs, including catechin/curcumin [3], EGCG/lycopene [4], EGCG/quercetin [2], vi-

tamin C/xanthoxylin [5], phycocyanin/astaxanthin [6], vitamin B12/Cydia pomonella granulovirus (CpGV) [7], and rivoflavin/ β -carotene [8].

Most DEs are stabilized using conventional emulsifiers, such as small synthetic surfactants, and predominantly biopolymers such as proteins and polysaccharides, since they migrate less from the outer to the inner droplets and form viscoelastic layers [1]. However, DEs stabilized with conventional emulsifiers are subject to several instability phenomena during both storage and gastrointestinal (GI) digestion, such as coalescence of oil droplets and W_1 droplets, the flux of water and water-soluble components between W_1 and W_2 , and migration of emulsifiers between both interfaces, among other mechanisms that trigger the release and degradation of the bioactive compounds encapsulated during oral or gastric digestion [9,10]. In this context, recent advancements have led to exploring alternative stabilizing agents, such as solid particles, to enhance the stability of DEs and their performance as delivery systems during digestion [9]. Pickering stabilization uses solid particles that irreversibly adsorb to the interface, forming a rigid barrier that prevents coalescence and reduces the loss of W_1 , enhancing the stability of DEs [11]. Biomaterial-based solid particles have gained great interest in recent years for stabilizing Pickering DEs, such as oligosaccharide and polysaccharide particles, water-insoluble protein particles, fat particles, or protein–polysaccharide conjugates [11]. Cellulose nanocrystals (CNCs), obtained from cellulose fibers by acid hydrolysis, are composed of linear chains of β -D-glucopyranose molecules bonded by hydrogen bonds, forming nanorods with diameters ranging from 5 to 70 nm in width and from 100 nm to several micrometers in length [12,13]. This biocompatible, sustainable, and biodegradable material can be used to stabilize Pickering o/w emulsions, as it exhibits a rod-like nanometric structure with a high aspect ratio and amphiphilic nature, allowing for irreversible adsorption at the O:W interface and the formation of a thick electrically charged coatings around oil droplets [11,14]. CNCs have been primarily used to stabilize simple o/w emulsions [12,15,16], where the stabilization effect depends on various factors such as its biological origin, concentration, surface charge and aspect ratio [15,17–20]. However, a limited number of studies have investigated the use of CNCs to stabilize the O:W₂ interface in DEs, either in their unmodified form or chemically modified, or by forming complexes with proteins [14,17,21]. These Pickering DEs have been reported to show high stability over time [17], high resistance to both heat and salt stress, and greater encapsulation stability [14]. To the best of our knowledge, there is only one study in which the performance of CNC-stabilized DEs has been evaluated as co-delivery vehicles for hydrophilic and hydrophobic bioactive compounds during GI digestion [14]. In that study, the use of protein fibrils and CNC complexes at the outer interface of DEs resulted in higher bioaccessibility of both hydrophilic and hydrophobic bioactive compounds.

This study focuses on the co-encapsulation of chlorogenic acid (CA) in W_1 and curcumin in the linseed oil phase of $W_1/O/W_2$ double emulsions. CA, abundant in coffee and tea, and curcumin, found in turmeric, exhibit numerous health benefits such as antioxidant and anti-inflammatory activity, among others [22,23]. However, curcumin's bioavailability is limited by its poor water solubility, chemical instability, and rapid metabolism [3], while CA's stability is affected by pH changes during digestion, resulting in low bioaccessibility values [24]. The outer interface of these DEs was stabilized with CNCs, providing an innovative approach to enhance the stability and functionality of these emulsions and to control the release of both bioactive compounds during *in vitro* gastrointestinal digestion.

The aim of this research was to assess the bioaccessibility of CA and curcumin simultaneously encapsulated in DEs with the outer interface stabilized using unmodified CNCs. Additionally, these Pickering DEs underwent characterization regarding droplet size, encapsulation efficiency, morphology, rheological properties, and creaming stability. A comparative analysis was conducted with DEs stabilized with sodium caseinate at the outer interface.

2. Materials and Methods

2.1. Materials

Chlorogenic acid (with a purity of 98%) was obtained from AK Scientific (Union City, CA, USA). Linseed oil was acquired from Nutra Andes Ltd. (Valparaíso, Chile). Curcumin (total curcuminoids > 95%) was sourced from Xi'an Xin Sheng Bio-Chem Co. (Xi'an, China). Cellulose nanocrystals (CNCs) obtained from cotton cellulose pulp via sulfuric acid hydrolysis were purchased in freeze-dried form from the Process Development Center of the University of Maine (Orono, ME, USA). Porcine bile extract (B8631) and digestive enzymes (pepsin from porcine gastric mucosa, P7012, 2500 AU/mg; pancreatin from porcine pancreas, P7545, 8× USP specifications) were purchased from Sigma-Aldrich (Santiago, Chile). Polyglycerolpolyricinoleate (PGPR) was acquired from Dimerco S.A. (Santiago, Chile). Sodium caseinate was sourced from Prinal S.A. (Santiago, Chile). Grupo Blumos (Santiago, Chile) donated the high methoxy pectin (Aglupectin HS-RAM).

2.2. Characterization of CNC

The ζ -potential, hydrodynamic size, and size distribution of CNCs were measured by laser Doppler velocimetry and dynamic light scattering (DLS), respectively, at 25 °C (Zetasizer Nano-ZS, Malvern Instruments, Worcestershire, UK). CNCs were previously dispersed in milli-Q water (0.1% *w/w*) with an ultrasonic processor (30 KHz, 100% amplitude) for 5 min. The ζ -potential of CNCs was also measured at pH 2 (-15.9 ± 0.9 mV) and pH 7 (-42.0 ± 1.8 mV), following dilution with water adjusted to the corresponding pH. Topographic images of CNCs were obtained by atomic force microscopy (AFM) in air-tapping mode at a frequency of 100 kHz using a high-resolution tip (model DP18/HiRes-C, mmasch, Watsonville, CA, USA). In this analysis, an aliquot of a CNC dispersion (1.5 g/L) was deposited on a mica substrate that was previously cleaved and conditioned at 20 °C. The sample was dried under a stream of nitrogen gas and placed in an AFM measuring cell (AFM Veeco, Plainview, NY, USA), where images were acquired using the software program Nanoscope AFM v6.13r1.

2.3. Formulation of Pickering DE-CNC

A two-step emulsification process was used to obtain the DEs. Initially, an ultrasonic processor (30 KHz, 100% amplitude, work time 1 s, rest time 1 s) was used for 3 min to prepare the W_1/O emulsions. CA was dissolved in the inner aqueous phase (W_1 ; 0.1% *w/w*). Linseed oil with curcumin (0.3% *w/w*) and PGPR (6% *w/w*) composed the oil phase. The $W_1:O$ ratio was 20:80. Subsequently, the W_1/O emulsion was slowly added, drop by drop, onto the W_2 , employing a rotor–stator homogenizer (Omni GLH 850, OMNI International, Kennesaw, GA, USA). The W_2 consisted of sodium azide (0.02% *w/w*) and CNCs (8.3% *w/w*) dispersed in deionized water using an ultrasonic processor (30 KHz, 100% amplitude) for 5 min. To optimize the homogenization conditions for DE-CNC, a central composite + star design was employed. The independent variables were homogenization speed (ranging from 5000 to 15,000 rpm) and homogenization time (from 1 to 15 min), while the response variables were the oil droplet size ($D_{4,3}$) of freshly prepared DEs and the creaming index after 7 days of storage at 4 °C (CI_7), which were determined as described in Section 2.4.1. The experimental data was fitted to a second-order regression model using the following equation (Equation (1)):

$$Y = b_0 + \sum_{i=1}^2 b_i X_i + \sum_{i=1}^2 b_{ii} X_i^2 + \sum_{i=1}^1 \sum_{j=i+1}^2 b_{ij} X_i X_j \quad (1)$$

where Y was the estimated response (CI_7 or $D_{4,3}$), subscript i and j ranged from 1 to 2 ($n = 2$), b_0 was the intercept term, b_i , b_{ii} , and b_{ij} values were the linear, quadratic, and interaction coefficients, respectively, and X_i and X_j were the levels of the independent variables.

In the equation, terms that were not statistically significant ($p > 0.05$) were eliminated, with the exception of linear forms of the homogenization speed or homogenization time, which are fundamental components of the mathematical model. The software program

Statgraphics Centurion XVI, version 16.2 (Statistical Graphics Corporation, Rockville, MD, USA) was used to perform the analysis of variance (ANOVA), lack-of-fit, and the determination of regression coefficients. The optimal conditions for each independent variable were determined by the response surface methodology (RSM). Multiple optimization of the response variables, where CI_7 and $D_{4,3}$ were minimized, was performed using the desirability function.

For comparison, a control DE (DE-NaCas) was prepared with W_2 containing sodium caseinate (NaCas, 0.5% *w/w*), high methoxy pectin (3% *w/w*), and sodium azide (0.02% *w/w*) in deionized water. The homogenization parameters for DE-NaCas were optimized in prior research (6000 rpm and 4.64 min). Consistently, the $W_1/O:W_2$ ratio was the same for all DEs (40:60). An osmometer (3320, Advanced Instruments, Norwood, MA, USA) was used to equilibrate the osmolarity of W_1 and W_2 .

2.4. Characterization of DEs Obtained under Optimal Conditions

2.4.1. Oil Droplet Size and Size Distribution, Microstructure, Creaming Stability, and ζ -Potential

The size distribution of oil droplets and volume mean diameter ($D_{4,3}$) were determined in freshly prepared DEs and after 21 days of storage at 4 °C. This was accomplished using light-scattering techniques with a particle analyzer (LA-960V2, Horiba, Kyoto, Japan). The refractive index of linseed oil, set at 1.479, was taken into account, and the samples were appropriately diluted in distilled water (at a ratio of 1:2500).

Confocal laser scanner microscopy (CLSM; LSM 700, Carl Zeiss Microscopy GmbH, Jena, Germany) was used to evaluate the microstructure of DEs at days 0 and 21 of storage at 4 °C. The oil phase was fluorescently labelled with Nile red (0.01% *w/w*; excitation and emission wavelengths of 488 nm and 580 nm, respectively). The CLSM images were analyzed with the ZEN 2012 (Blue Edition, Carl Zeiss Microscopy GmbH, Jena, Germany) software.

A vertical scan analyzer (Turbiscan, MA2000, Formulaction, Toulouse, France) was used to assess the creaming stability of DEs at regular intervals throughout a 21-day storage period at 4 °C. The creaming index (CI) was calculated from the backscattering profiles according to the following equation (Equation (2)):

$$\text{Creaming Index} = \frac{HS}{HE} \times 100 \quad (2)$$

where HS is the height of the serum layer, and HE is the total height of the DE.

A Zetasizer Nano ZS instrument (Malvern Instruments Ltd., Worcestershire, UK) was employed to evaluate the ζ -potential of the freshly prepared DEs at 25 °C by laser Doppler velocimetry. The DEs were appropriately diluted with water adjusted to a pH of 7 (1:2500 *v/v*).

2.4.2. Encapsulation Efficiency of CA and Curcumin in DEs

The concentration of CA and curcumin in the W_2 phase of fresh DEs was quantified to determine the encapsulation efficiency (EE) of the bioactive compounds in DEs [25]. This was accomplished using an UPLC system (UltiMate 3000, Thermo Fisher Scientific, Waltham, MA, USA) coupled with a UV/VIS detector (VWD-3100). Following gentle centrifugation at $2400 \times g$ for 15 min, the W_2 phase containing the non-encapsulated CA and curcumin was isolated and injected into the UPLC system. The concentration of CA was determined according to [26] (Epic C18, 250×4.6 mm, 5 μm ; Perkin Elmer, Waltham, MA, USA), while curcumin concentration was determined according to [27] (Acquity BEH shield RP18, 130 Å, 2.1 mm \times 100 mm, 1.7 μm ; Waters, Milford, MA, USA). Standard calibration curves (0.1–100 $\mu\text{g/mL}$; $R^2 = 0.99$ in both cases) were used for quantification of both bioactive compounds. The following equation (Equation (3)) was used to calculate the EE:

$$EE(\%) = 100 - \frac{C_{w2} \times 100}{C_0} \quad (3)$$

where C_{W_2} was the concentration of CA or curcumin recovered in W_2 , and C_0 was the initial total concentration of CA or curcumin in the DEs.

2.4.3. Rheological Properties

Rheological measurements were conducted on fresh DEs using a Discovery Hybrid Rheometer (HR-1, TA Instruments, New Castle, DE, USA), equipped with a cone-plate geometry (60 mm diameter, 1° angle, 29 μm gap). DE samples were carefully loaded onto the measuring system and allowed to rest for 5 min to facilitate structure recovery and temperature equilibration. An increasing shear rate from 0.01 to 1000 s^{-1} at 25 $^\circ\text{C}$ was applied to determine the viscosity of each DE, and the apparent viscosity (Pa·s) was recorded as a function of the shear rate.

2.5. Bioaccessibility of CA, Curcumin, Total Free Fatty Acids (FFA) and Major FFA

DEs were subjected to a standardized *in vitro* gastrointestinal digestion [28], simulating oral, gastric, and intestinal phase conditions. Simulated salivary fluid (4 mL), distilled water (4.375 mL), and 0.3 M CaCl_2 (25 μL) were added to freshly prepared DE (1.6 g) for the oral phase. Since none of the samples contained amylase-sensitive polysaccharides, no amylases were added. The mixture was adjusted to pH 7.0 and incubated at 37 $^\circ\text{C}$ with continuous shaking at 170 rpm for 2 min. Following this, the bolus obtained after the oral phase was mixed with the simulated gastric fluid (8 mL), pepsin (2000 U/mL gastric phase), and HCl (0.1 M) to achieve a pH of 2.0, 0.3 M CaCl_2 (5 μL), and distilled water up to 20 mL. The mixture was incubated at 37 $^\circ\text{C}$ under continuous shaking at 170 rpm for 120 min. Afterward, the gastric chyme (20 mL) was mixed with the simulated intestinal fluid (16 mL), 0.3 M CaCl_2 (40 μL), NaOH (1 M) to adjust pH to 7.0, bile extract (10 mM), and pancreatin (2000 U lipase activity/mL intestinal phase) to simulate the intestinal phase. The pH was maintained at 7.0 for 2 h at 37 $^\circ\text{C}$ by the addition of NaOH (1 M) under constant stirring using a pH-stat (902 Titrando, Metrohm, Herisau, Switzerland).

Optical microscopy (DM500, Leica Microsystems, Germany) was used to evaluate the microstructure of DEs following each digestion phase. The amount of CA and curcumin released following the oral and gastric phase was assessed by quantifying the concentration of bioactive compounds in the aqueous phase of each gastrointestinal *in vitro* digestion phase as described in Section 2.4.2. To quantify the release of CA and curcumin following the intestinal phase, the digested material was subjected to centrifugation ($7500 \times g$ for 60 min) to collect the micellar phase (aqueous phase), and the concentration of CA and curcumin was assessed following the procedure outlined in Section 2.4.2.

The retrieval of free fatty acids (FFA) liberated during the intestinal phase followed the procedure described by [29]. FFA were methylated using a solution of $\text{H}_2\text{S}_2\text{O}_4$ in methanol (0.06% *v/v*), and the resulting fatty acid methyl esters (FAMES) were subjected to gas chromatography analysis (7890B, Agilent Technologies, Santa Clara, CA, USA) as detailed by Álvarez et al. [30]. Gas chromatography was equipped with a flame ionization detector and an HP-88 column (fused silica capillary column with 0.25 mm inner diameter, 0.20 μm film thickness, and 100 m length, Agilent Technologies, Santa Clara, CA, USA). Individual fatty acids were identified and quantified with calibration curves generated with FAME external standards ($R^2 > 0.99$ for all of them). The bioaccessibility of CA, curcumin, and every major FFA was determined using Equation (4).

$$\text{Bioaccessibility}(\%) = 100 - (C_{AD}/C_i) \times 100 \quad (4)$$

where C_{AD} was the concentration of CA, curcumin, or FFA in the micellar phase after the intestinal phase of digestion and C_i was the concentration of CA, curcumin, or FFA in the undigested DE.

2.6. Statistical Analysis

All experiments were conducted in triplicate. Statistical analysis was performed using ANOVA and Tukey's multiple range test to determine statistically significant differences

($p \leq 0.05$) among samples. Data analysis was carried out using Statgraphics Centurion XVI software, version 16.2 (Statistical Graphics Corporation, Rockville, MD, USA).

3. Results and Discussion

3.1. Characterization of CNC

The particle size distribution and microstructure of CNCs are shown in Figure 1. The CNCs presented a bimodal particle size distribution ranging from 9 to 200 nm (Figure 1A) and a Z-average of 64.74 ± 1.27 nm. The polydispersity index was 0.250 ± 0.007 . The broad range of particle sizes suggests the presence of particles of varying sizes within the dispersion. However, the microstructure of the CNCs, as observed in AFM images (Figure 1B), revealed rod-shaped crystals measuring 100–200 nm in length and approximately 10–20 nm in width. This observation explains the wide distribution obtained with the DLS method, as DLS measures particle size from any angle, approximating a spherical shape.

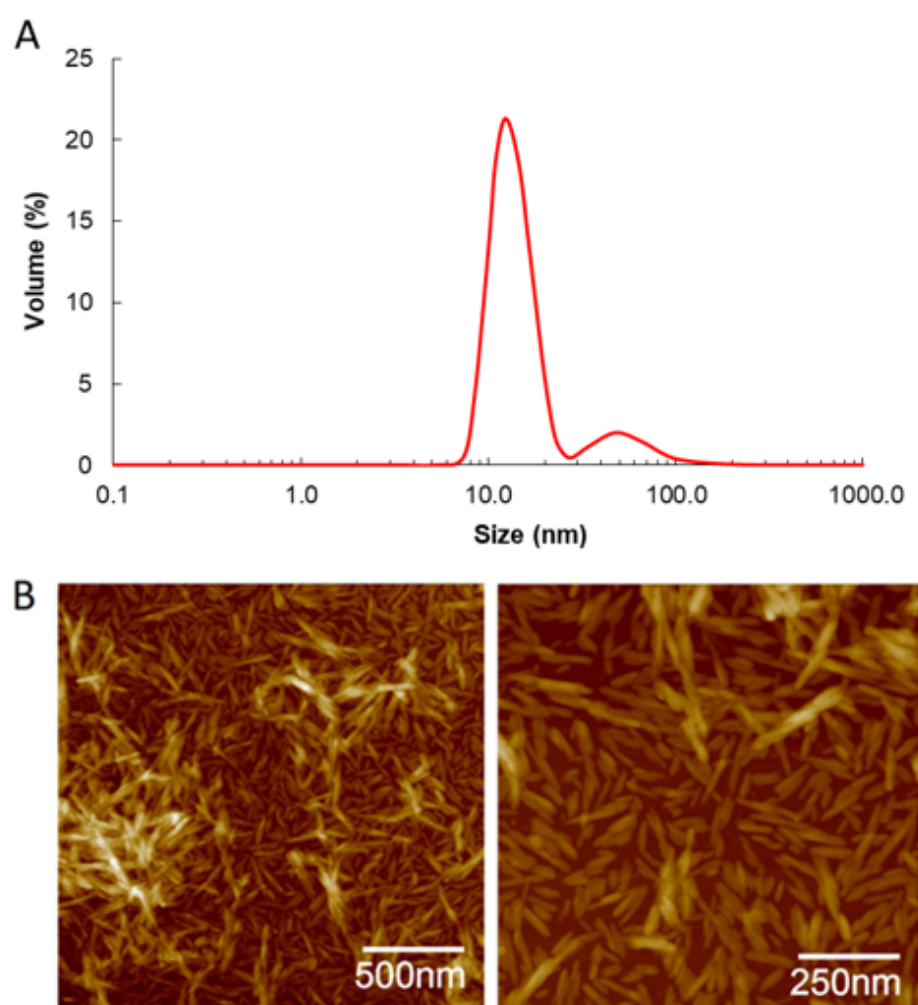


Figure 1. Particle size distribution measured by DLS (A) and AFM topographic images (B) of CNC.

The sizes observed in the AFM images fall within the range described in the literature for CNC, usually ranging from 5 to 70 nm in width and from 75 nm to several micrometers in length [12,13]. The ζ -potential of CNCs was -41.8 ± 1.4 mV, attributed to the presence of negatively charged sulfate groups at its surface as a consequence of the processing conditions involving sulfuric acid hydrolysis [31]. This elevated ζ -potential value is expected to prevent the coalescence of oil droplets due to the electrostatic repulsion generated by the CNCs adsorbed at the outer interface of DE-CNC.

3.2. Optimal DE-CNC Homogenization Parameters

Table 1 displays the central composite + star design alongside the ANOVA results pertaining to the preparation of DE-CNC.

Table 1. Central composite + star design and ANOVA for the preparation of DE-CNC.

Run	HS (rpm) (X_1)	HT (min) (X_2)	Droplet Size ($D_{4,3}$) (μm)	CI_7
1	11,000	16.4	26.15 \pm 0.36	5.91 \pm 0.10
2	5000	8.5	42.33 \pm 1.00	9.35 \pm 0.83
3	6000	2.0	42.16 \pm 0.51	6.34 \pm 0.15
4	16,000	8.5	24.77 \pm 0.20	8.27 \pm 0.54
5	15,000	15.0	25.48 \pm 0.13	11.89 \pm 0.93
6	15,000	2.0	24.72 \pm 0.13	5.62 \pm 0.21
7	6000	15.0	32.69 \pm 0.19	5.53 \pm 0.17
8	11,000	0.6	29.85 \pm 0.35	5.57 \pm 0.23
9	11,000	8.5	26.83 \pm 0.11	6.09 \pm 0.31
10	11,000	8.5	25.00 \pm 0.15	4.55 \pm 0.19
11	11,000	8.5	25.36 \pm 0.09	5.98 \pm 0.56
12	11,000	8.5	26.62 \pm 0.03	5.65 \pm 0.43
ANOVA	Droplet size ($D_{4,3}$) (μm)		CI_7	
	Estimate	<i>p</i> -value	Estimate	<i>p</i> -value
β_0	77.88		19.24	
X_1	−0.0071	0.0003 *	−0.0024	0.0948
X_1^2	2.31×10^{-7}	0.0117 *	9.80×10^{-8}	0.0094 *
X_2	−1.21	0.0008 *	−0.5070	0.0479 *
X_1X_2	8.74×10^{-5}	0.0111 *	6.07×10^{-5}	0.0141 *
Lack of fit		0.236		0.113
R^2 (adj. for d.f.)		96.31		65.18

HS: homogenization speed; HT: homogenization time; CI_7 : creaming index after 7 days of storage at 4 °C; adj. for d.f.: adjusted for degrees of freedom. β_0 : intercept term; X_1 : Homogenization speed; X_2 : homogenization time; X_1X_2 : interaction between HS and HT. Data are average \pm standard deviation (n = 3).

The $D_{4,3}$ of freshly prepared DEs and CI_7 were in the range of 24.7–42.3 μm and 4.6–11.9%, respectively. The linear forms of both the homogenization time and speed, the quadratic form of the homogenization speed and the interaction form of homogenization time and speed were significant ($p < 0.05$) for both $D_{4,3}$ and CI_7 . The model explained 96.3% and 65.2% of the variability (R^2 adjusted by degrees of freedom) in $D_{4,3}$ and CI_7 , respectively, and the lack of fit was not significant ($p > 0.05$) in any case. The response surface graphics (Figure 2A–C) showed that the higher the homogenization speed, the smaller the droplet size, especially at short homogenization times (Figure 2A). This is because higher speed results in greater shear force applied, which promotes the reduction of oil droplet size. Regarding the CI_7 (Figure 2B), at short homogenization times, the percentage of creaming tended to increase as the homogenization speed decreased, which may be because insufficient energy is applied during such a short period to generate small droplets, thus promoting creaming. However, at longer homogenization times, the percentage of creaming tended to increase with increasing speed, suggesting that an excess of shear force may induce some emulsion breaking and favor creaming.

The desirability function was used for the multiple optimization of the response variables, where both $D_{4,3}$ and CI_7 were minimized (Figure 2C). The highest desirability value (0.98) was achieved with 13,599 rpm and 0.63 min, which were adjusted to 13,000 rpm and 1 min for practical reasons. Under these optimal conditions, the predicted values for $D_{4,3}$ and CI_7 by the model were 24.5 μm and 4.5%, respectively.

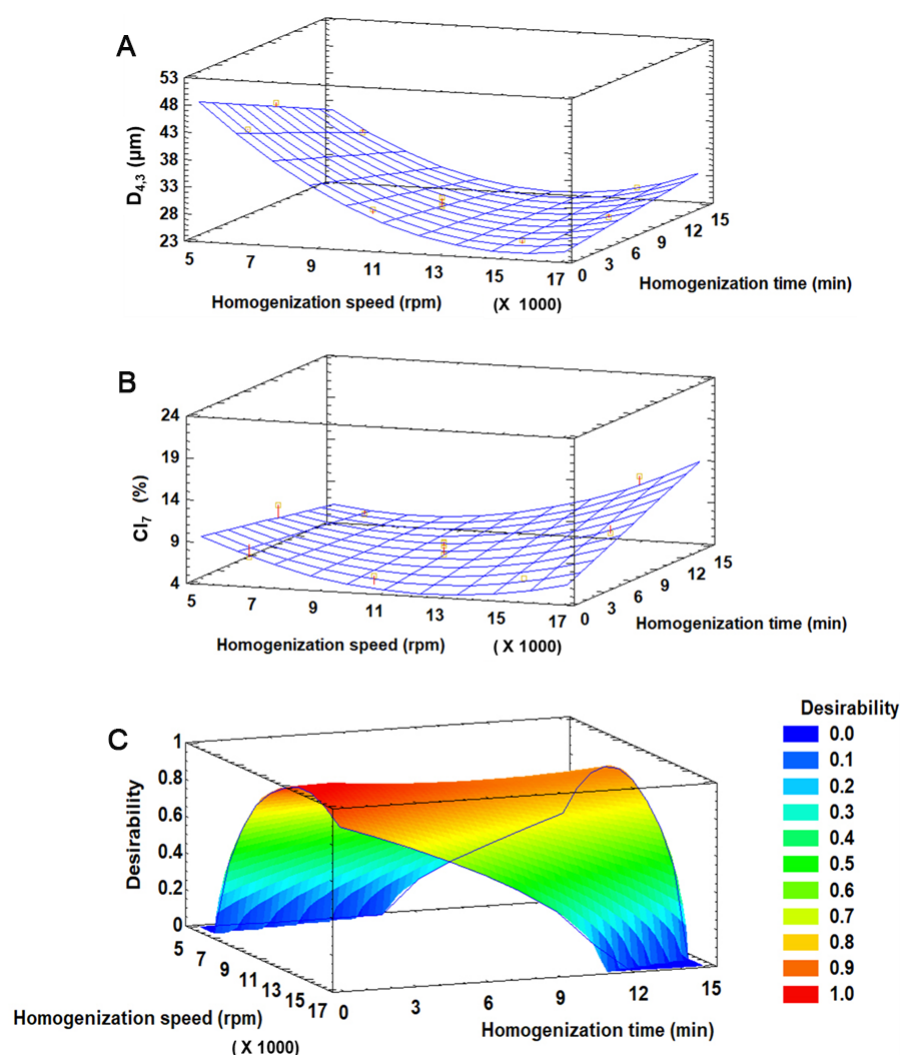


Figure 2. Response surface graphics for $D_{4,3}$ (A), IC_7 (B), and desirability function (C) for the preparation of DE-CNC.

3.3. Characterization of DEs Obtained under Optimal Conditions

3.3.1. Oil Droplet Size and Size Distribution, Microstructure, Creaming Stability, and ζ -Potential

Both DE-CNC and DE-NaCas showed a bimodal size distribution (Figure 3), with a larger oil droplet population with sizes between 10 and 100 μm , and a smaller oil droplet population with sizes between 0.8 and 4–5 μm . At day 0 of storage, DE-CNC displayed the smallest droplet size (~ 20 μm), while DE-NaCas exhibited a significantly ($p < 0.05$) larger $D_{4,3}$ value (~ 25 μm). After 21 days of storage at 4 $^{\circ}\text{C}$, a slight but significant increase in droplet size was observed for DE-CNC ($p < 0.05$), reaching approximately 27 μm , indicating some degree of oil droplet coalescence. Other studies [14,21] showed larger oil droplet sizes (50–100 μm) in DEs stabilized with CNC, likely due to the utilization of lower CNC concentrations in W_2 (1.5 and 3.8 wt% vs. 8.3 wt%). Conversely, CNCs with similar characteristics than those employed in this study in terms of size and ζ -potential were utilized at 0.3 wt% for stabilizing o/w simple emulsions obtained by sonication [12], resulting in smaller oil droplet sizes (3 μm). Besides the type and concentration of emulsifiers, emulsification method, as well as the density and viscosity of the phases, may also influence oil droplet size [32].

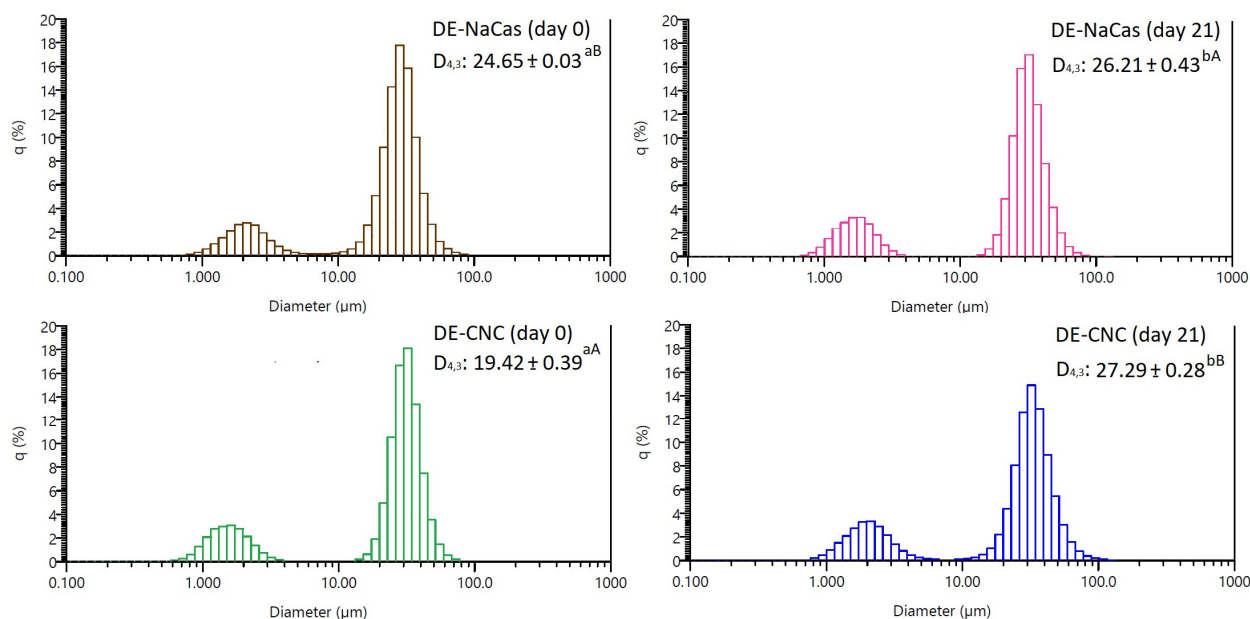


Figure 3. The distribution of oil droplet sizes, and $D_{4,3}$ values of freshly prepared DE-NaCas and DE-CNC, and after 21 days of storage at 4 °C. Different uppercase letters (A, B) denote significant differences ($p < 0.05$) observed among DE samples at the same storage period. Different lowercase letters (a, b) represent significant differences ($p < 0.05$) observed for the same sample over the course of storage.

Figure 4 shows the microstructure of DE-CNC obtained under optimal conditions and the control DE-NaCas at days 0 and 21 of storage at 4 °C. On day 0, both DE-CNC and DE-NaCas showed the characteristic multicompartimentalized structure representing DEs, with small water droplets inside the oil droplets that are dispersed in the W_2 . However, noticeable increases in the size of W_1 droplets were observed in DE-NaCas after 21 days of storage, accompanied by a greater abundance of small oil droplets (Figure 3) that can be observed in the oil droplet size distribution but did not affect the $D_{4,3}$ values, probably because this parameter is sensitive to the presence of large particles within a polydisperse system [33]. The changes observed in DE-NaCas may be attributed to the occurrence of coalescence among W_1 inner droplets and their migration into W_2 . Regarding DE-CNC, minimal changes were observed in their microstructure during storage. A slight enlargement in oil droplet size was observed after 21 days of storage, aligning with the rise in $D_{4,3}$ values. Nevertheless, the formation of compact CNC layers on the surface of oil droplets, created through strong interactions among CNC nanoparticles via van der Waals and hydrogen bonding [34], resulted in the retention of the multicompartimentalized structure, with no observable changes in the size of the W_1 droplets.

Emulsions exhibit resistance to droplet aggregation by maintaining a high surface potential, which is closely associated with the ζ -potential, a measure of surface charge. This results in robust electrostatic repulsion among the droplets, effectively preventing their coalescence [16]. Both DE-CNC and DE-NaCas initially exhibited highly negative ζ -potential values of -44.1 ± 5.4 and -35.7 ± 0.3 mV, respectively, indicating favorable initial stability for both emulsions [16]. In the case of DE-CNC, the low ζ -potential values closely resembled those of CNC (-41.8 ± 1.35 mV), indicating that the electrostatic repulsion among DE-CNC oil droplets is governed by the surface potential of CNC, attributed to the presence of hydroxyl and sulfate groups [31]. Conversely, the highly negative values observed in DE-NaCas can be attributed to the negative charge of ionized carboxyl groups present in caseinate and pectin [35]. A decrease in the absolute value of ζ -potential during storage may affect the emulsion stability, as colloidal systems are prone to flocculate when ζ -potential approaches zero [36]. At day 21 of storage, both DEs showed ζ -potential values

close to their initial ones (-43.4 ± 3.0 mV for DE-CNC and -38.6 ± 0.9 mV for DE-NaCas), which contributes to the high creaming stability found up to day 21 of storage (Figure 5).

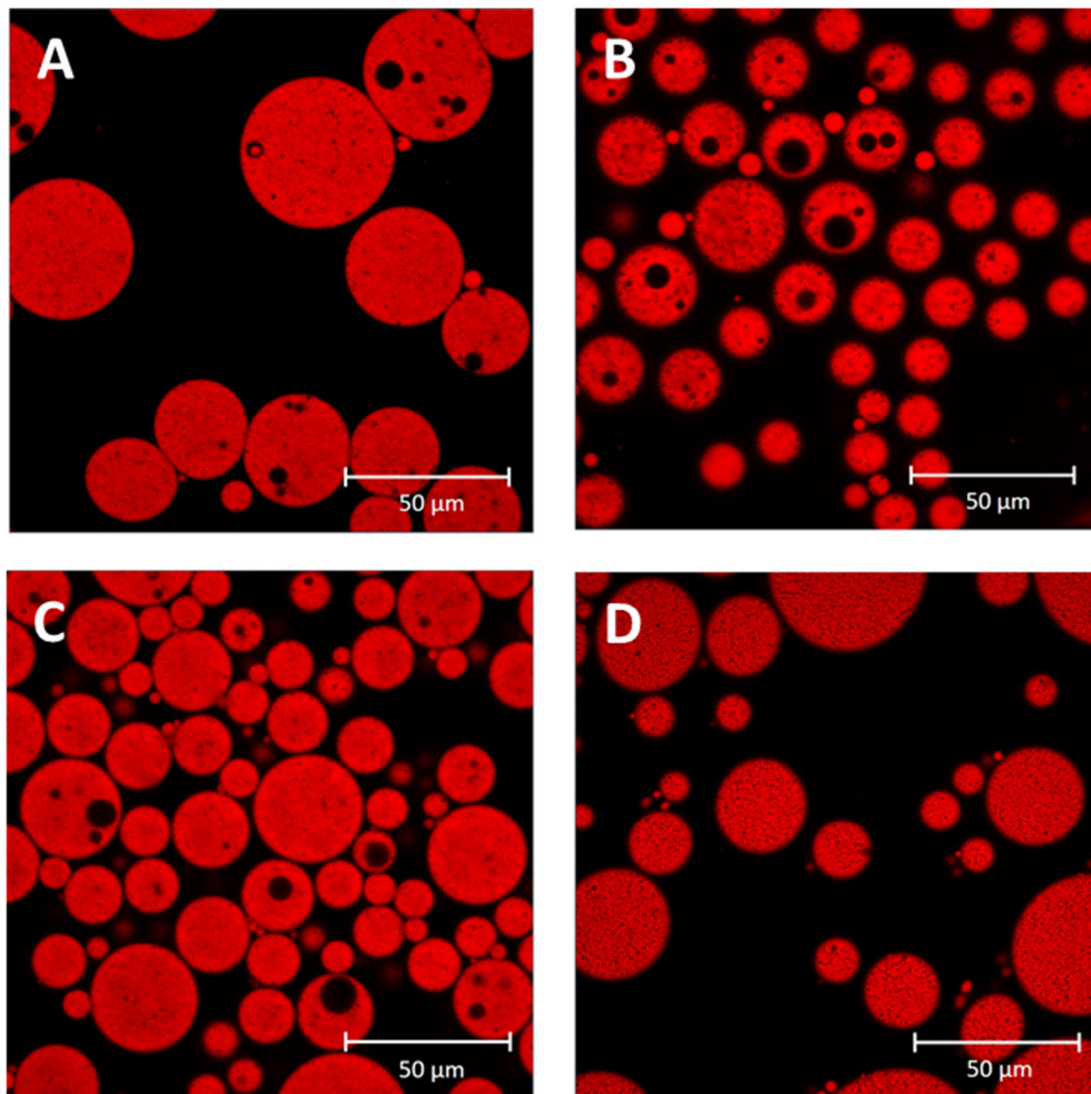


Figure 4. Confocal laser scanning microscopy (CLSM) of DE-NaCas ((A), day 0; (B), day 21) and DE-CNC ((C), day 0; (D), day 21).

In the natural aging process of a W/O/W emulsion, similar to other emulsified systems, changes in appearance and structure may occur due to creaming induced by gravity and macroscopic phase separation [36]. The CI values for days 0, 7, 14, 21, and 42 of storage at 4 °C for both DE-CNC and DE-NaCas are depicted in Figure 5. Initially, both DE-CNC and DE-NaCas exhibited CI below 7% and 5%, respectively, with no significant differences ($p < 0.05$) observed. Over 21 days of storage at 4 °C, neither emulsion showed notable increases in creaming ($p > 0.05$), showing values lower than 7%. Pectin, recognized for its stabilizing properties in o/w emulsions due to its ability to increase the viscosity of the continuous phase and hinder the upward movement of oil droplets [37,38], contributed to the stability of DE-NaCas during storage. In the case of DE-CNC, the CNC not adsorbed at the interface and present in the continuous phase may enhance the viscosity of W_2 through the formation of a gel-like network, restricting the ascent of oil droplets [39,40]. Furthermore, the highly negative ζ -potential values found in both DEs during storage are associated with the high creaming stability observed, despite the presence of droplets larger than 25 μm , which typically promotes creaming. However, after 42 days of storage,

significant differences ($p < 0.05$) in creaming stability were observed, with DE-NaCas exhibiting a CI of $23.75 \pm 1.48\%$, whereas DE-CNC showed a CI of $6.79 \pm 0.16\%$ (Figure 5). This suggests that despite the increased viscosity and electrostatic repulsive forces in DE-NaCas, the stabilization mechanism with this conventional emulsifier does not provide long-term creaming stability. This could be attributed to the fact that CNCs not only generate electrostatic repulsive forces between the droplets but also create strong steric forces, thereby enhancing their resistance to aggregation during a prolonged storage time [16].

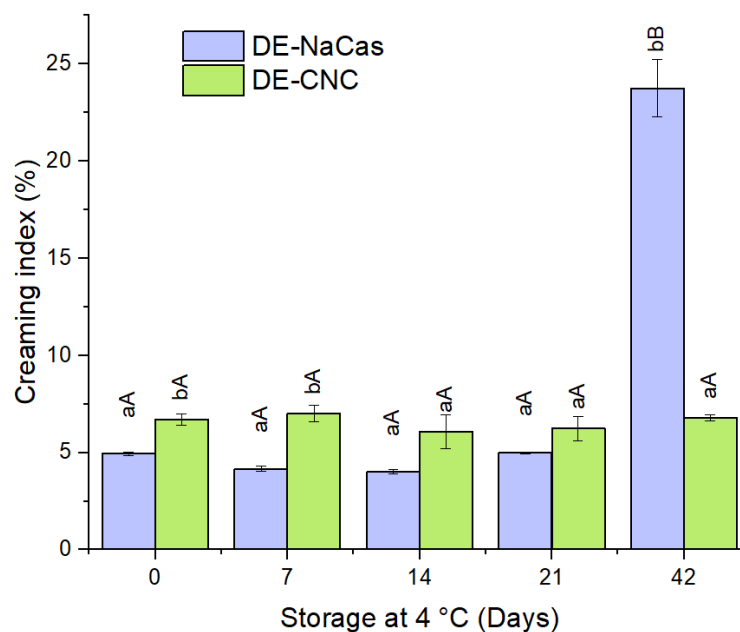


Figure 5. Creaming index (CI) (%) of DE-NaCas and DE-CNC stored 21 days at 4 °C. Distinct lowercase letters (a, b) denote significant differences ($p < 0.05$) observed between DEs at identical storage times. Different uppercase letters (A, B) denote significant differences ($p < 0.05$) for the same DE throughout the storage period.

3.3.2. Encapsulation Efficiency of CA and Curcumin

The EE of CA, representing the percentage of CA retained within W_1 droplets, was significantly higher ($p < 0.05$) in DE-CNC ($92.6 \pm 0.9\%$) than in DE-NaCas ($23.7 \pm 2.7\%$). Despite similar microstructural features (Figure 4), suggesting comparable W_1 content, the EE indicates that CA migrated from W_1 to W_2 during homogenization, possibly through the oil phase and both DE interfaces. The use of solid particles as emulsion stabilizers, specifically CNC in this case, provides enhanced stability due to their adsorption at the oil droplet surface, forming a compact layer at the interface [40]. In general, it has been reported that particles with appropriate wettability characteristics and sizes greater than approximately 10 nm irreversibly adsorb to the O:W interface [41]. Cui et al. [14] also reported EE close to 90% for hydrophilic epigallocatechin gallate in DEs stabilized by protein fibrils and CNC at the outer interface. Other studies employing other solid particles to stabilize the outer interface in DEs, such as chemically modified quinoa starch granules, have also reported high values of EE for the hydrophilic bioactive compound encapsulated in W_1 ($\sim 98.5\%$), highlighting the ability of solid particles to retain W_1 and the encapsulated compounds within it [42]. Reports indicate that EE values of CA in DEs depend on the emulsion composition [43]. These authors encapsulated CA in DEs of linseed oil stabilized with conventional emulsifiers. The highest EE values for CA (84–88%) were found in DEs stabilized with a mixture of Span 80 and lecithin as lipophilic emulsifier, Tween 20 as hydrophilic emulsifier, and containing chitosan in W_1 and/or W_2 .

Regarding the EE of curcumin, both DEs exhibited high EE values without significant differences between them ($98.6 \pm 0.1\%$ for DE-NaCas and $97.4 \pm 0.1\%$ for DE-CNC;

$p > 0.05$), owing to its lipophilic nature ($\log P = 3.10$ [3]), which prevents curcumin from migrating to either of the two aqueous phases (W_1 or W_2). Similarly, high EE values of curcumin (approximately 88%) have also been reported in DEs stabilized with conventional emulsifiers (PGPR and Tween 80) [3]. Curcumin has also been encapsulated in DEs stabilized by Pickering mechanism, although studies are limited. For instance, it has been reported a high EE of curcumin (approximately 97%) in emulsion droplets with the $O:W_2$ interface stabilized by whey protein fibrils or by whey protein fibrils and CNC complexes [14].

3.3.3. Rheological Properties

The flow curve recorded at 25 °C for both studied DEs is presented in Figure 6. Although both DEs showed similar initial viscosity at the onset of the shear rate sweeping (1 Pa·s at 0.02 s^{-1}), DE-NaCas showed higher viscosity values than DE-CNC across the entire range of tested shear rates, due to the viscosity imparted by 3% pectin in W_2 . The presence of pectin leads to a higher effective volume fraction of the dispersed phase due to its relatively large and flexible structure. Additionally, pectin molecules can interact with each other through hydrophobic interactions and hydrogen bonding, contributing to the high observed viscosity [37]. The viscosity of CNC-stabilized Pickering emulsions is attributed to the formation of a three-dimensional network between nanoparticles and water molecules by van der Waals forces, electrostatic forces, and hydrogen bonds [44]. Both DEs presented a non-Newtonian behavior, with viscosity values decreasing as the shear rate increased, depicting a pseudoplastic behavior. Interestingly, in the case of DE-CNC, three regions were distinguished in the flow curve: a shear thinning regime at low strain ($<0.1 \text{ s}^{-1}$), a Newtonian-plateau at strain values within the range $1\text{--}10 \text{ s}^{-1}$, and a further decrease in viscosity at strains above 100 s^{-1} . This rheological behavior has been described as typical for lyotropic liquid crystals [45] and has been previously reported in CNC suspensions [46] and CNC-stabilized emulsions [44]. Herein, the shear thinning behavior could be explained by the alignment of the chiral domains of the liquid crystal in the flow direction, and revealing that interaction between oil phase, water phase and solid emulsifier were weak [44]. This behavior has been previously observed in Pickering emulsions due to the absence of any chemical bonds [44]. The Newtonian-plateau would be related with the CNC concentration, suggesting that CNC-stabilized DEs may undergo microstructure change at higher shear rates [47].

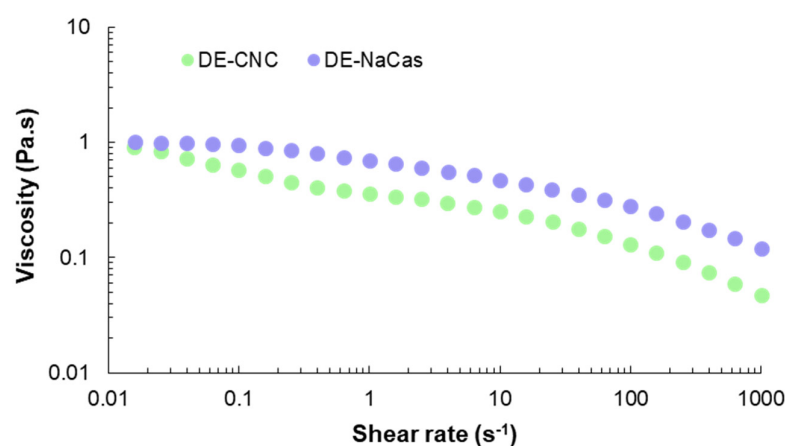


Figure 6. Flow curve of DE-CNC and DE-NaCas.

3.4. Release of CA and Curcumin from DEs during In Vitro Gastrointestinal Digestion

The microstructure of DE-CNC and DE-NaCas, alongside the percentage of curcumin and CA released following each phase of the in vitro gastrointestinal digestion, is displayed in Figure 7. As inferred from the EE values of CA, the concentration of CA in the W_2 of freshly prepared DE-CNC and DE-NaCas was $7.4 \pm 0.9\%$ and $76.3 \pm 2.7\%$, respectively.

Post-oral digestion, a significant release of CA was observed in both DEs, approximately 15% for DE-CNC and 9% for DE-NaCas, reaching $22.3 \pm 0.2\%$ and $84.9 \pm 3.8\%$ of CA released at the end of the oral phase, respectively. Despite coalescence occurring in both DEs (Figure 7(A1,A2)), numerous W_1 droplets were present in DE-CNC, while DE-NaCas had few water droplets, correlating with the released CA percentages.

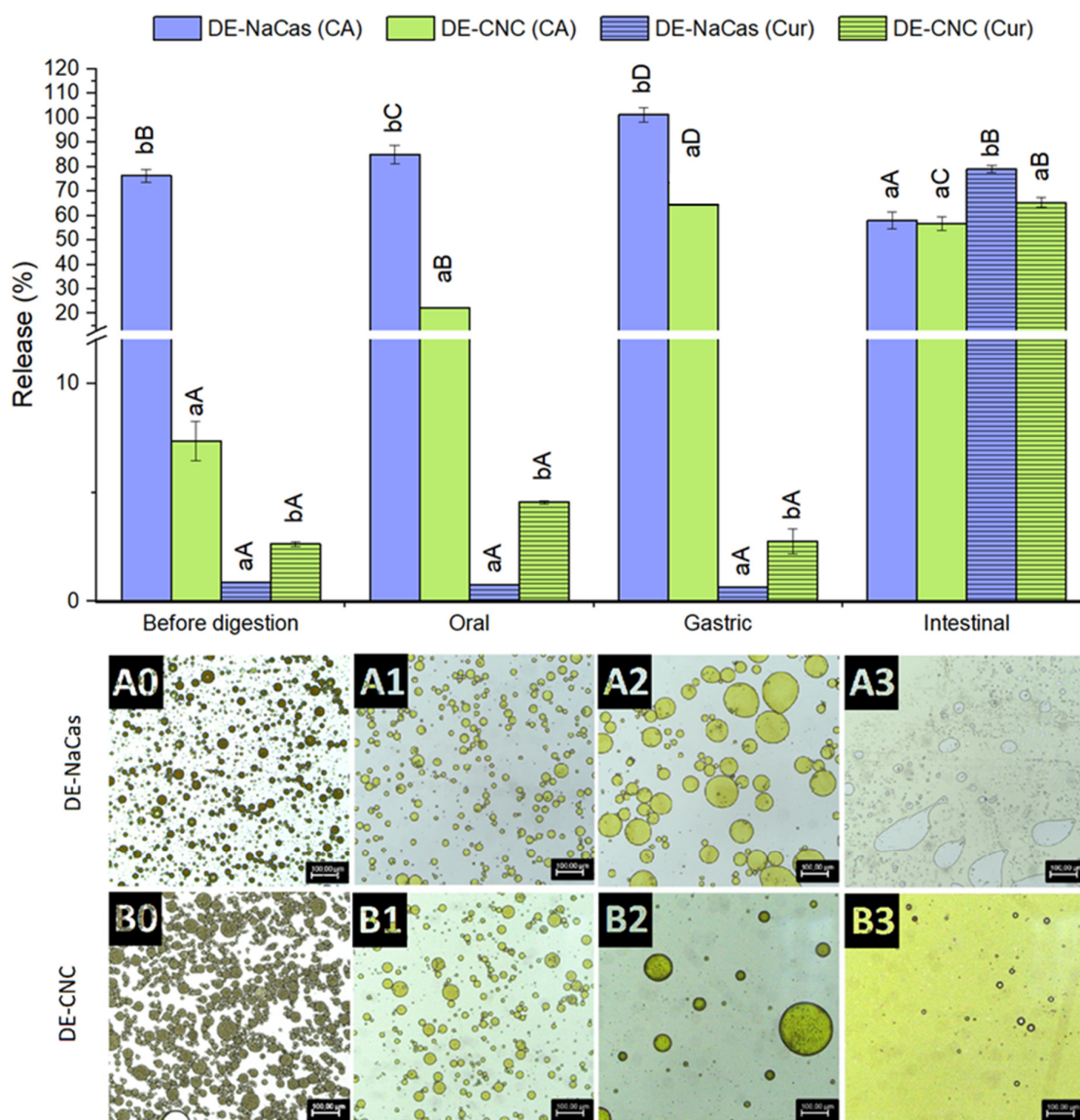


Figure 7. CA and curcumin released from DE-NaCas and DE-CNC before digestion and after oral, gastric, and intestinal phases of an in vitro gastrointestinal digestion. Microstructure of DEs (A: DE-NaCas and B: DE-CNC) before (0), and after oral (1), gastric (2), and intestinal (3) phases of an in vitro gastrointestinal digestion. Different lowercase letters (a, b) indicate significant differences ($p < 0.05$) among DEs for the same phase of digestion. Different uppercase letters (A–D) indicate significant differences ($p < 0.05$) among the different digestion phases for the same sample.

During the gastric phase, a substantial release of CA occurred in both DEs (Figure 7), reaching $64.0 \pm 1.6\%$ in DE-CNC and complete release in DE-NaCas ($101.3 \pm 3.0\%$). In the case of DE-NaCas, coalescence was the most significant microstructural change in oil droplets (Figure 7(A2)), possibly due to sodium caseinate hydrolysis by pepsin. Coalescence and loss of round contours were observed in DE-CNC oil droplets, but still maintained the typical multicompartimentalized structure with numerous water droplets inside the

oil droplets (Figure 7(B2)), suggesting that CA was mainly released by diffusion due to osmotic effects in this phase. This coalescence may result from a weakened electrostatic repulsion between oil droplets due to the gastric phase of digestion being performed at pH 2, at which CNC exhibited a low ζ -potential (-15.9 ± 0.9) as a consequence of the partial protonation of covalently bound sulfate ester groups ($pK_a = 1.9$) [48]. Additionally, the high ionic strength of the gastric fluids may lead to electrostatic screening, contributing to a reduction in the electrostatic repulsion of oil droplets [49,50]. Sharkar et al. [51] formulated o/w emulsions using a composite layer of whey protein and CNCs as stabilizers. They observed that the presence of CNC enhanced the resistance of the interfacial protein film to pepsin hydrolysis, thus inhibiting droplet coalescence during the gastric phase. However, it is important to note that this digestion took place at pH 3, where CNC exhibited a high ζ -potential (-43.8 mV) and had the capability to bind with positively charged whey protein, leading to the formation of a rigid composite protein–particle layer. In other study, Cui et al. [14] formulated DEs stabilized by whey protein isolate fibrils and CNC complexes at the outer interface, as co-delivery systems of curcumin and epigallocatechin gallate. These DEs experienced some coalescence of individual oil droplets and exhibited loss of their round shape after gastric phase, which was conducted at pH 2.5. However, the percentage of epigallocatechin gallate release from the DEs after the gastric phase was not reported.

After the intestinal phase of digestion, the bioaccessible fraction of CA was around 57–58% in both DEs (Figure 7), and no significant differences ($p > 0.05$) were found between DE-NaCas ($58.0 \pm 3.4\%$) and Pickering DE-CNC ($56.8 \pm 2.8\%$). In the case of DE-NaCas, CA underwent partial degradation during the intestinal phase, given its low stability at pH 7 [52], since CA had been completely released in the gastric phase and thus exposed to the adverse intestinal conditions. In the case of DE-CNC, there was both a release of CA that remained trapped in W_1 , due to the collapse of the DE structure observed as a result of the action of lipases on the triacylglycerides present in the oil phase, and a degradation of CA exposed to digestion conditions. As shown in Figure 7(A3,B3), the complete destruction of the DEs structure was observed after 2 h of *in vitro* intestinal digestion, characterized by the appearance of free oil following the breakdown of the emulsion. These findings suggest that the use of CNC-stabilized DEs facilitated a consistent release of CA throughout the oral, gastric, and intestinal phases of digestion. These bioaccessibility values notably surpassed those documented in other studies ($\sim 18\%$ [53]; $\sim 23\%$ [24]; $\sim 35\%$ [54]), indicating the protective function of DEs in maintaining CA stability during *in vitro* digestion. This could be attributed to the potential entrapment of CA within the formed micelles during the intestinal phase [3].

The release of curcumin during simulated digestion phases is shown in Figure 7. During oral and gastric digestion, curcumin release to W_2 was below 1% in DE-NaCas, while DE-CNC showed a slightly higher ($p < 0.05$) release, reaching $2.76 \pm 0.58\%$ after the gastric phase. In any case, the percentage of curcumin released to the W_2 phase during the oral and gastric phases in both DEs was much lower than the percentage of CA released during the same digestion stages, owing to the lipophilic nature of curcumin.

During the intestinal phase, the triglycerides in the flaxseed oil, which constitute the oil phase of the DE, were hydrolyzed by the lipases present in pancreatin, leading to the release of curcumin dissolved in the oil and its incorporation into the mixed micelles formed from bile salts and fatty acids. The DE-CNC exhibited significantly lower ($p < 0.05$) curcumin bioaccessibility values ($65.3 \pm 2.0\%$) than DE-NaCas ($79.1 \pm 1.5\%$). The reduced curcumin release in the case of DE-CNC at the intestinal level can be attributed to the presence of CNC around the oil droplets, which may hinder the access of lipases as reported in O/W emulsions stabilized with CNC [46,49]. However, it has also been described that nanometric CNC rods leave uncovered spaces on the surface of the oil droplets due to non-aligned adsorption to the interface [15]. These spaces allow bile salts and lipases to access the oil droplets [46,55], explaining the bioaccessibility values obtained for curcumin in the DE-CNCs that can still be considered high ($65.3 \pm 2.0\%$). These values were comparable to those reported by Cui et al. [14] for the bioaccessibility of curcumin (68.9%) when co-

encapsulated with epigallocatechin gallate in DEs stabilized by whey protein isolate fibrils and CNC complexes at the outer interface.

3.5. Bioaccessibility of Total Free Fatty Acids and Individual FFA

The fatty acids released after the intestinal phase of digestion were used to evaluate the extent of DE lipolysis. Figure 8 shows the bioaccessibility of the total FFA and the major individual fatty acids at the end of the intestinal phase of the *in vitro* gastrointestinal digestion of DE-CNC and DE-NaCas. Although the bioaccessibility of the total FFA in DE-CNC and DE-NaCas was statistically similar ($p > 0.05$), the values tended to be lower in DE-CNC ($49.91 \pm 0.77\%$) than in DE-NaCas ($59.54 \pm 5.17\%$), suggesting that CNC may hinder lipase access to the oil droplets, in line with the lower bioaccessibility values observed for curcumin. A significantly lower extent of lipolysis has been reported in other studies where CNC-stabilized o/w emulsions have been subjected to *in vitro* digestion. This has been attributed to the CNC irreversibly adsorbed to oil droplets, which limits the adsorption of bile salts and lipases [49].

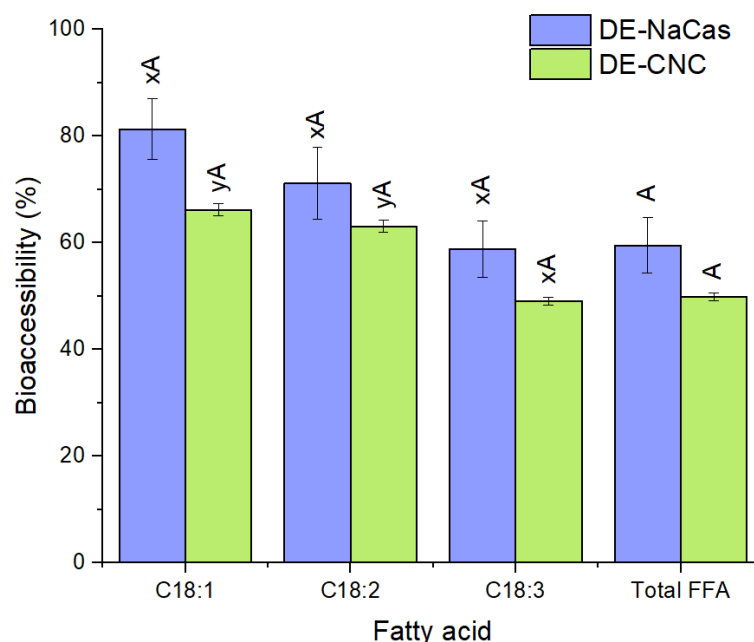


Figure 8. Total FFA and major individual FFA bioaccessibility (%) at the end of the *in vitro* gastrointestinal digestion of DE-CNC and DE-NaCas. Distinct uppercase letters (A, B) denote significant differences ($p < 0.05$) between samples for the same fatty acid. Distinct lowercase letters (x, y) denote significant differences ($p < 0.05$) among fatty acids for the same DE.

In both digested DEs, a trend towards reduced bioaccessibility of the major individual FFA was observed with an increase in the degree of unsaturation of the fatty acids (Figure 8), aligning with the results obtained in other studies where the bioaccessibility of the major fatty acids from linseed oil tended to decrease from C18:1 to C18:3 [56]. This effect has been related to the enzymatic activity of lipases, which tend to preferentially hydrolyze less unsaturated fatty acids because there is a greater distance between the first double bond and the ester bond in the fatty acid chain [57]. Additionally, less unsaturated fatty acids may be more effectively incorporated into mixed micelles due to their higher hydrophobicity [57], which would also explain the observed trend in the bioaccessibility of the major fatty acids from linseed oil in this study.

4. Conclusions

The outer interface of DEs, designed as co-delivery systems of CA and curcumin, was successfully stabilized with CNC in this study. These Pickering DEs resulted in

a noticeably higher EE for the hydrophilic bioactive compound (CA) and were more resistant to creaming than conventional DEs stabilized with sodium caseinate in the outer interface, showing good storage stability. These effects may be attributed to the formation of compact layers of CNC around the oil droplets, resulting in electrostatic and steric repulsion between the oil droplets, as well as to the restriction of the oil droplets movement due to the viscosity imparted by CNC. They ensured a consistent CA release throughout digestion and facilitated the intestinal release of curcumin, resulting in notable bioaccessibility values for both CA and curcumin. CNC-stabilized DEs could thus represent a promising approach for the simultaneous oral delivery of hydrophilic CA and hydrophobic curcumin.

Author Contributions: Methodology, J.P.-T., J.H. and P.D.-C.; investigation, J.P.-T. and J.H.; writing—original draft preparation, J.P.-T., P.D.-C., P.R. and B.G.; writing—review and editing, J.P.-T., P.D.-C., P.R. and B.G.; conceptualization, B.G.; supervision, B.G.; project administration, B.G.; funding acquisition, B.G. All authors have read and agreed to the published version of the manuscript.

Funding: This research was funded by ANID (FONDECYT Project 1210909 and National Doctoral Grant 212111012).

Data Availability Statement: The data presented in this study are available on request from the corresponding author.

Acknowledgments: Authors thank the support and scientific expertise of Leonardo Caballero and Francisco Melo (Department of Physics, University of Santiago, Chile).

Conflicts of Interest: The authors declare no conflicts of interest.

References

1. Øye, G.; Simon, S.; Rustad, T.; Paso, K. Trends in Food Emulsion Technology: Pickering, Nano-, and Double Emulsions. *Curr. Opin. Food Sci.* **2023**, *50*, 101003. [[CrossRef](#)]
2. Chen, X.; McClements, D.J.; Wang, J.; Zou, L.; Deng, S.; Liu, W.; Yan, C.; Zhu, Y.; Cheng, C.; Liu, C. Coencapsulation of (-)-Epigallocatechin-3-Gallate and Quercetin in Particle-Stabilized W/O/W Emulsion Gels: Controlled Release and Bioaccessibility. *J. Agric. Food Chem.* **2018**, *66*, 3691–3699. [[CrossRef](#)] [[PubMed](#)]
3. Aditya, N.P.; Aditya, S.; Yang, H.; Kim, H.W.; Park, S.O.; Ko, S. Co-Delivery of Hydrophobic Curcumin and Hydrophilic Catechin by a Water-in-Oil-in-Water Double Emulsion. *Food Chem.* **2015**, *173*, 7–13. [[CrossRef](#)] [[PubMed](#)]
4. Wang, Q.; Wang, L.; Abdullah, N.; Tian, W.; Song, M.; Cao, Y.; Xiao, J. Co-Delivery of EGCG and Lycopene via a Pickering Double Emulsion Induced Synergistic Hypolipidemic Effect. *Food Funct.* **2022**, *13*, 3419–3430. [[CrossRef](#)] [[PubMed](#)]
5. Wang, R.; Ma, C.; Yan, H.; Wang, P.; Yu, S.; Zhang, T.; Yin, Z. Preparation and Characterization of GX-50 and Vitamin C Co-Encapsulated Microcapsules by a Water-in-Oil-in-Water (W1/O/W2) Double Emulsion-Complex Coacervation Method. *Langmuir* **2023**, *39*, 13863–13875. [[CrossRef](#)] [[PubMed](#)]
6. Zhang, P.; Sun, Y.; Hou, Y.; Wang, H.; Tan, M. Fabrication of Novel W/O/W Emulsion Gels Using Beeswax Stabilized W/O: Preparation, Characterization and Co-Delivery of Phycocyanin and Astaxanthin. *Food Biosci.* **2023**, *57*, 103536. [[CrossRef](#)]
7. Nollet, M.; Laurichesse, E.; Schmitt, V. Double Emulsions Stabilized by PGPR and Arabic Gum as Capsules: The Surprising Stabilizing Role of Inner Droplets. *Langmuir* **2023**, *40*, 1646–1657. [[CrossRef](#)] [[PubMed](#)]
8. Zhao, S.; Deng, X.; Wang, Y.; Chen, S.; Liu, X.; Liu, F. Co-Delivery of Hydrophobic β -Carotene and Hydrophilic Riboflavin by Novel Water-in-Oleic Acid-in-Water (W/OA/W) Emulsions. *Food Chem.* **2024**, *432*, 137224. [[CrossRef](#)] [[PubMed](#)]
9. Luo, T.; Wei, Z. Recent Progress in Food-Grade Double Emulsions: Fabrication, Stability, Applications, and Future Trends. *Food Front.* **2023**, *4*, 1622–1642. [[CrossRef](#)]
10. McClements, D.J. Encapsulation, Protection, and Release of Hydrophilic Active Components: Potential and Limitations of Colloidal Delivery Systems. *Adv. Colloid. Interface Sci.* **2015**, *219*, 27–53. [[CrossRef](#)] [[PubMed](#)]
11. Zhang, J.; Zhu, J.; Cheng, Y.; Huang, Q. Recent Advances in Pickering Double Emulsions and Potential Applications in Functional Foods: A Perspective Paper. *Foods* **2023**, *12*, 992. [[CrossRef](#)] [[PubMed](#)]
12. Zhang, H.; Qian, Y.; Chen, S.; Zhao, Y. Physicochemical Characteristics and Emulsification Properties of Cellulose Nanocrystals Stabilized O/W Pickering Emulsions with High -OSO₃- Groups. *Food Hydrocoll.* **2019**, *96*, 267–277. [[CrossRef](#)]
13. Kaboorani, A.; Riedl, B. Surface Modification of Cellulose Nanocrystals (CNC) by a Cationic Surfactant. *Ind. Crops Prod.* **2015**, *65*, 45–55. [[CrossRef](#)]
14. Cui, F.; Han, S.; Wang, J.; McClements, D.J.; Liu, X.; Liu, F. Co-Delivery of Curcumin and Epigallocatechin Gallate in W/O/W Emulsions Stabilized by Protein Fibril-Cellulose Complexes. *Colloids Surf. B Biointerfaces* **2023**, *222*, 113072. [[CrossRef](#)] [[PubMed](#)]
15. Kalashnikova, I.; Bizot, H.; Cathala, B.; Capron, I. New Pickering Emulsions Stabilized by Bacterial Cellulose Nanocrystals. *Langmuir* **2011**, *27*, 7471–7479. [[CrossRef](#)] [[PubMed](#)]

16. Han, S.; Cui, F.; McClements, D.J.; Ma, C.; Wang, Y.; Wang, X.; Liu, X.; Liu, F. Enhancing Emulsion Stability and Performance Using Dual-Fibrous Complexes: Whey Protein Fibrils and Cellulose Nanocrystals. *Carbohydr. Polym.* **2022**, *298*, 120067. [[CrossRef](#)] [[PubMed](#)]
17. Cunha, A.G.; Mougel, J.B.; Cathala, B.; Berglund, L.A.; Capron, I. Preparation of Double Pickering Emulsions Stabilized by Chemically Tailored Nanocelluloses. *Langmuir* **2014**, *30*, 9327–9335. [[CrossRef](#)]
18. Kalashnikova, I.; Bizot, H.; Cathala, B.; Capron, I. Modulation of Cellulose Nanocrystals Amphiphilic Properties to Stabilize Oil/Water Interface. *Biomacromolecules* **2012**, *13*, 267–275. [[CrossRef](#)] [[PubMed](#)]
19. Kalashnikova, I.; Bizot, H.; Bertoncini, P.; Cathala, B.; Capron, I. Cellulosic Nanorods of Various Aspect Ratios for Oil in Water Pickering Emulsions. *Soft Matter* **2013**, *9*, 952–959. [[CrossRef](#)]
20. Zhu, M.; Huan, S.; Liu, S.; Li, Z.; He, M.; Yang, G.; Liu, S.; McClements, D.J.; Rojas, O.J.; Bai, L. Recent Development in Food Emulsion Stabilized by Plant-Based Cellulose Nanoparticles. *Curr. Opin. Colloid. Interface Sci.* **2021**, *56*, 101512. [[CrossRef](#)]
21. Zhu, W.; Ma, W.; Li, C.; Pan, J.; Dai, X. Well-Designed Multihollow Magnetic Imprinted Microspheres Based on Cellulose Nanocrystals (CNCs) Stabilized Pickering Double Emulsion Polymerization for Selective Adsorption of Bifenthrin. *Chem. Eng. J.* **2015**, *276*, 249–260. [[CrossRef](#)]
22. Santana-Gálvez, J.; Cisneros-Zevallos, L.; Jacobo-Velázquez, D.A. Chlorogenic Acid: Recent Advances on Its Dual Role as a Food Additive and a Nutraceutical against Metabolic Syndrome. *Molecules* **2017**, *22*, 358. [[CrossRef](#)] [[PubMed](#)]
23. Sharifi-Rad, J.; Rayess, Y.E.; Rizk, A.A.; Sadaka, C.; Zgheib, R.; Zam, W.; Sestito, S.; Rapposelli, S.; Neffe-Skocińska, K.; Zielińska, D.; et al. Turmeric and Its Major Compound Curcumin on Health: Bioactive Effects and Safety Profiles for Food, Pharmaceutical, Biotechnological and Medicinal Applications. *Front. Pharmacol.* **2020**, *11*, 550909. [[CrossRef](#)] [[PubMed](#)]
24. Alongi, M.; Calligaris, S.; Anese, M. Fat Concentration and High-Pressure Homogenization Affect Chlorogenic Acid Bioaccessibility and α -Glucosidase Inhibitory Capacity of Milk-Based Coffee Beverages. *J. Funct. Foods* **2019**, *58*, 130–137. [[CrossRef](#)]
25. Silva, W.; Torres-Gatica, M.F.; Oyarzun-Ampuero, F.; Silva-Weiss, A.; Robert, P.; Cofrades, S.; Giménez, B. Double Emulsions as Potential Fat Replacers with Gallic Acid and Quercetin Nanoemulsions in the Aqueous Phases. *Food Chem.* **2018**, *253*, 71–78. [[CrossRef](#)] [[PubMed](#)]
26. Qi, W.; Zhao, T.; Yang, W.W.; Wang, G.H.; Yu, H.; Zhao, H.X.; Yang, C.; Sun, L.X. Comparative Pharmacokinetics of Chlorogenic Acid after Oral Administration in Rats. *J. Pharm. Anal.* **2011**, *1*, 270–274. [[CrossRef](#)] [[PubMed](#)]
27. Marczylo, T.H.; Steward, W.P.; Gescher, A.J. Rapid Analysis of Curcumin and Curcumin Metabolites in Rat Biomatrices Using a Novel Ultraperformance Liquid Chromatography (UPLC) Method. *J. Agric. Food Chem.* **2009**, *57*, 797–803. [[CrossRef](#)] [[PubMed](#)]
28. Brodkorb, A.; Egger, L.; Alming, M.; Alvito, P.; Assunção, R.; Ballance, S.; Bohn, T.; Bourlieu-Lacanal, C.; Boutrou, R.; Carrière, F.; et al. INFOGEST Static In vitro Simulation of Gastrointestinal Food Digestion. *Nat. Protoc.* **2019**, *14*, 991–1014. [[CrossRef](#)] [[PubMed](#)]
29. Ng, N.; Chen, P.X.; Ghazani, S.M.; Wright, A.J.; Marangoni, A.; Goff, H.D.; Joye, I.J.; Rogers, M.A. Lipid Digestion of Oil-in-Water Emulsions Stabilized with Low Molecular Weight Surfactants. *Food Funct.* **2019**, *10*, 8195–8207. [[CrossRef](#)] [[PubMed](#)]
30. Álvarez, R.; Giménez, B.; Mackie, A.; Torcello-Gómez, A.; Quintriqueo, A.; Oyarzun-Ampuero, F.; Robert, P. Influence of the Particle Size of Encapsulated Chia Oil on the Oil Release and Bioaccessibility during In vitro Gastrointestinal Digestion. *Food Funct.* **2022**, *13*, 1370–1379. [[CrossRef](#)] [[PubMed](#)]
31. Lin, N.; Dufresne, A. Nanocellulose in Biomedicine: Current Status and Future Prospect. *Eur. Polym. J.* **2014**, *59*, 302–325. [[CrossRef](#)]
32. Heidari, F.; Jafari, S.M.; Ziaifar, A.M.; Malekjani, N. Stability and Release Mechanisms of Double Emulsions Loaded with Bioactive Compounds; a Critical Review. *Adv. Colloid. Interface Sci.* **2022**, *299*, 102567. [[CrossRef](#)] [[PubMed](#)]
33. McClements, D.J. *Food Emulsions: Principles, Practices, and Techniques*, 3rd ed.; CRC Press: Boca Raton, FL, USA, 2015.
34. Pandey, A.; Derakhshandeh, M.; Kedzior, S.A.; Pilapil, B.; Shomrat, N.; Segal-Peretz, T.; Bryant, S.L.; Trifkovic, M. Role of Interparticle Interactions on Microstructural and Rheological Properties of Cellulose Nanocrystal Stabilized Emulsions. *J. Colloid. Interface Sci.* **2018**, *532*, 808–818. [[CrossRef](#)] [[PubMed](#)]
35. Verkempinck, S.H.E.; Kyomugasho, C.; Salvia-Trujillo, L.; Denis, S.; Bourgeois, M.; Van Loey, A.M.; Hendrickx, M.E.; Grauwet, T. Emulsion Stabilizing Properties of Citrus Pectin and Its Interactions with Conventional Emulsifiers in Oil-in-Water Emulsions. *Food Hydrocoll.* **2018**, *85*, 144–157. [[CrossRef](#)]
36. Muschiolik, G.; Dickinson, E. Double Emulsions Relevant to Food Systems: Preparation, Stability, and Applications. *Compr. Rev. Food Sci. Food Saf.* **2017**, *16*, 532–555. [[CrossRef](#)] [[PubMed](#)]
37. Liu, J.; Zhou, H.; Tan, Y.; Muriel Mundo, J.L.; McClements, D.J. Comparison of Plant-Based Emulsifier Performance in Water-in-Oil-in-Water Emulsions: Soy Protein Isolate, Pectin and Gum Arabic. *J. Food Eng.* **2021**, *307*, 110625. [[CrossRef](#)]
38. Ngouémazong, E.D.; Christiaens, S.; Shpigelman, A.; Van Loey, A.; Hendrickx, M. The Emulsifying and Emulsion-Stabilizing Properties of Pectin: A Review. *Compr. Rev. Food Sci. Food Saf.* **2015**, *14*, 705–718. [[CrossRef](#)]
39. Wang, W.; Du, G.; Li, C.; Zhang, H.; Long, Y.; Ni, Y. Preparation of Cellulose Nanocrystals from Asparagus (*Asparagus officinalis* L.) and Their Applications to Palm Oil/Water Pickering Emulsion. *Carbohydr. Polym.* **2016**, *151*, 1–8. [[CrossRef](#)]
40. Aw, Y.Z.; Lim, H.P.; Low, L.E.; Surjit Singh, C.K.; Chan, E.S.; Tey, B.T. Cellulose Nanocrystal (CNC)-Stabilized Pickering Emulsion for Improved Curcumin Storage Stability. *LWT* **2022**, *159*, 113249. [[CrossRef](#)]
41. Yusoff, A.; Murray, B.S. Modified Starch Granules as Particle-Stabilizers of Oil-in-Water Emulsions. *Food Hydrocoll.* **2011**, *25*, 42–55. [[CrossRef](#)]

42. Matos, M.; Timgren, A.; Sjö, M.; Dejmeck, P.; Rayner, M. Preparation and Encapsulation Properties of Double Pickering Emulsions Stabilized by Quinoa Starch Granules. *Colloids Surf. A Physicochem. Eng. Asp.* **2013**, *423*, 147–153. [[CrossRef](#)]
43. Dima, C.; Dima, S. Water-in-Oil-in-Water Double Emulsions Loaded with Chlorogenic Acid: Release Mechanisms and Oxidative Stability. *J. Microencapsul.* **2018**, *35*, 584–599. [[CrossRef](#)] [[PubMed](#)]
44. Li, Z.; Jiang, X.; Yao, Z.; Chen, F.; Zhu, L.; Liu, H.; Ming, L. Chitosan Functionalized Cellulose Nanocrystals for Stabilizing Pickering Emulsion: Fabrication, Characterization and Stability Evaluation. *Colloids Surf. A Physicochem. Eng. Asp.* **2022**, *632*, 127769. [[CrossRef](#)]
45. Onogi, S.; Asada, T. Rheology and Rheo-Optics of Polymer Liquid Crystals. In *Rheology*; Astarita, G., Marrucci, G., Nicolais, L., Eds.; Springer: Boston, MA, USA, 1980. [[CrossRef](#)]
46. Shafiei-Sabet, S.; Hamad, W.Y.; Hatzikiriakos, S.G. Rheology of Nanocrystalline Cellulose Aqueous Suspensions. *Langmuir* **2012**, *28*, 17124–17133. [[CrossRef](#)] [[PubMed](#)]
47. Miao, C.; Mirvakili, M.N.; Hamad, W.Y. A Rheological Investigation of Oil-in-Water Pickering Emulsions Stabilized by Cellulose Nanocrystals. *J. Colloid. Interface Sci.* **2022**, *608*, 2820–2829. [[CrossRef](#)] [[PubMed](#)]
48. Varanasi, S.; Henzel, L.; Mendoza, L.; Prathapan, R.; Batchelor, W.; Tabor, R.; Garnier, G. Pickering emulsions electrostatically stabilized by cellulose nanocrystals. *Front. Chem.* **2018**, *6*, 409. [[CrossRef](#)] [[PubMed](#)]
49. Bai, L.; Lv, S.; Xiang, W.; Huan, S.; McClements, D.J.; Rojas, O.J. Oil-in-Water Pickering Emulsions via Microfluidization with Cellulose Nanocrystals: 2. In Vitro Lipid Digestion. *Food Hydrocoll.* **2019**, *96*, 709–716. [[CrossRef](#)]
50. Bai, L.; Lv, S.; Xiang, W.; Huan, S.; McClements, D.J.; Rojas, O.J. Oil-in-Water Pickering Emulsions via Microfluidization with Cellulose Nanocrystals: 1. Formation and Stability. *Food Hydrocoll.* **2019**, *96*, 699–708. [[CrossRef](#)]
51. Sarkar, A.; Zhang, S.; Murray, B.; Russell, J.A.; Boxal, S. Modulating *In vitro* Gastric Digestion of Emulsions Using Composite Whey Protein-Cellulose Nanocrystals Interfaces. *Colloids Surf. B Biointerfaces* **2017**, *158*, 137–146. [[CrossRef](#)] [[PubMed](#)]
52. Narita, Y.; Inouye, K. Degradation Kinetics of Chlorogenic Acid at Various PH Values and Effects of Ascorbic Acid and Epigallocatechin Gallate on Its Stability under Alkaline Conditions. *J. Agric. Food Chem.* **2013**, *61*, 966–972. [[CrossRef](#)] [[PubMed](#)]
53. Yu, H.; Jeon, H.; Myeong, J.; Kwon, C.W.; Chang, P.S. Influence of Creamer Addition on Chlorogenic Acid Bioaccessibility and Antioxidant Activity of Instant Coffee during *In vitro* Digestion. *LWT* **2021**, *151*, 112178. [[CrossRef](#)]
54. Pollini, L.; Juan-García, A.; Blasi, F.; Mañes, J.; Cossignani, L.; Juan, C. Assessing Bioaccessibility and Bioavailability *In vitro* of Phenolic Compounds from Freeze-Dried Apple Pomace by LC-Q-TOF-MS. *Food Biosci.* **2022**, *48*, 101799. [[CrossRef](#)]
55. Ruiz-Rodríguez, P.E.; Meshulam, D.; Lesmes, U. Characterization of Pickering O/W Emulsions Stabilized by Silica Nanoparticles and Their Responsiveness to *In Vitro* Digestion Conditions. *Food Biophys.* **2014**, *9*, 406–415. [[CrossRef](#)]
56. Ramírez-Carrasco, P.; Alemán, A.; González, E.; Gómez-Guillén, M.C.; Robert, P.; Giménez, B. Bioaccessibility, Intestinal Absorption and Anti-Inflammatory Activity of Curcuminoids Incorporated in Avocado, Sunflower, and Linseed Beeswax Oleogels. *Foods* **2024**, *13*, 373. [[CrossRef](#)] [[PubMed](#)]
57. Costa, S.; Afonso, C.; Cardoso, C.; Batista, I.; Chaveiro, N.; Nunes, M.L.; Bandarra, N.M. Fatty Acids, Mercury, and Methylmercury Bioaccessibility in Salmon (*Salmo salar*) Using an *In Vitro* Model: Effect of Culinary Treatment. *Food Chem.* **2015**, *185*, 268–276. [[CrossRef](#)] [[PubMed](#)]

Disclaimer/Publisher’s Note: The statements, opinions and data contained in all publications are solely those of the individual author(s) and contributor(s) and not of MDPI and/or the editor(s). MDPI and/or the editor(s) disclaim responsibility for any injury to people or property resulting from any ideas, methods, instructions or products referred to in the content.